ELSEVIER

Thin Solid Films 387 (2001) 246–250

thin solid films

www.elsevier.com/locate/tsf

TEM, AFM, and cathodoluminescence characterization of CdTe thin films

M.M. Al-Jassim[a,*], Y. Yan[a], H.R. Moutinho[a], M.J. Romero[b], R.D. Dhere[a], K.M. Jones[a]

[a] *National Renewable Energy Laboratory, Golden, CO 80401, USA*
[b] *Departamento de Ciencia de los Materiales e I.M. y Q.I., Facultad de Ciencias, Universidad de Cádiz, Apdo. 40, E-11510, Puerto Real (Cádiz), Spain*

Abstract

The morphology, microstructure, and luminescent properties of polycrystalline CdTe films were investigated. The films were deposited by close-spaced sublimation at relatively low temperatures. The evolution of the film morphology and microstructure was studied as a function of deposition temperature and post-deposition heat treatment. Films deposited at low temperature exhibited fine, equiaxed grains. Dramatic grain growth was observed as a consequence of heat treatment. The film microstructure is heavily faulted and strongly dependent on the deposition and post-deposition treatment temperatures. The extended defects are mostly lamellar twins and stacking faults with similar densities. These defects often form a closely spaced arrangement, which leads to the formation of a local hexagonal phase. The presence of this hexagonal phase is expected to have significant effects on the electrical properties of the cubic CdTe films.

Keywords: CdTe; Solar cells; Transmission electron microscopy (TEM); Cathodoluminescence (CL); Atomic force microscopy (AFM)

1. Introduction

The CdTe/CdS system offers one of the most promising photovoltaic devices for terrestrial applications, due to the near-optimum bandgap and high absorption coefficient of CdTe. Polycrystalline, thin-film CdTe/CdS solar cells have demonstrated an efficiency of 15.8% [1]. However, as-deposited CdTe films exhibit very poor electrical characteristics [2]. In device fabrication, one of the process steps critical to achieving high efficiency is a post-deposition heat treatment in $CdCl_2$. The beneficial effect of this step indicates that defects in the as-grown CdTe films have profound effects on the electrical and optical properties of the material. Although post-deposition $CdCl_2$ heat treatment is critical, its role remains ambiguous. It was reported that the density of extended defects, mainly planar faults, in CdTe films decreases after the treatment [3]. However, our previous work showed little difference in the density of structural defects after such treatment [4]. We believe that to fully understand the role of the post-deposition heat treatment, we must understand the nature, density, and recombination behavior of these extended defects, and how such parameters change with the treatment. Furthermore, it is crucial to develop a good understanding of the film morphology, its dependence on the deposition and post-deposition conditions, and its effects on device performance.

Most investigations of defects in CdTe have so far focused on epitaxially grown films, and the reported extended defects are mainly lamellar twins [5,6]. However, epitaxially grown films generally have a different microstructure compared to close-spaced sublimation (CSS)-grown polycrystalline CdTe thin films, which are commonly used for CdTe/CdS solar cells [7]. In this

* Corresponding author. Tel.: +1-303-384-6602; fax: +1-303-384-6604.
E-mail address: mo@nrel.gov (M.M. Al-Jassim).

0040-6090/01/$ - see front matter
PII: S0040-6090(00)01707-7

paper, we report on the evolution of the morphology and microstructure of CSS-deposited CdTe. Additionally, we present data on the recombination characteristics of the defects, as investigated by cathodoluminescence (CL). Electron-beam injection techniques, such as CL, are well suited for resolving the electrical activity of individual grains in CdTe films, as shown by Galloway et al. [8,9].

2. Experimental

The structure of the cells used in this work was glass/SnO_2 (0.5 μm)/CdS (1000 Å)/CdTe (6 μm). The glass substrate was 7059 glass from Corning (borosilicate). The CdTe films were deposited by CSS at 620 and 450°C (hereafter, HT and LT for high- and low-temperature, respectively). The HT deposition was performed for comparison purposes. A post-deposition heat treatment with $CdCl_2$ was carried out using a novel $CdCl_2$ vapor treatment. The samples were treated in $CdCl_2$ vapor in the presence of a He and O_2 mixture (420/80 torr) for 5 min at temperatures varying from 400 to 450°C. The $CdCl_2$ source was a $CdCl_2$ film, previously deposited on a glass substrate by CSS, which was heated at the same temperature as the samples during the treatment. Details of the cells used in this study are shown in Table 1. The CdTe film morphology was studied by atomic force microscopy (AFM) using an Autoprobe CP from ThermoMicroscopes. The microstructure of the films was investigated by transmission electron microscopy (TEM). The TEM images were taken on a Philips CM30 microscope with a Cs = 2.0, operating at 300 kV. The CL experiments were carried out in a scanning electron microscope (SEM) at temperatures between 50 and 300 K, while the electron beam energy (E_b) was varied from 5 to 30 keV. The CL was collected using a semi-parabolic mirror attached to an optical guide. A cryogenic CCD (Photometrics SDS9000) was attached to an Oriel 77400 spectrograph/monochromator for spectroscopic measurements.

3. Results and discussion

Fig. 1 shows AFM images of as-deposited LT and HT CdTe films. The LT film (Fig. 1a) exhibits small grains with equiaxed grain morphology. The grain size is of the order of 0.3 μm. However, these small grains seem to agglomerate to form larger grains. Careful examination revealed that this is caused by the underlying large-grain SnO_2 film. HT films (Fig. 1b) exhibited a drastically different morphology. The grain size is in the 2–5 μm range, which is an order of magnitude higher than in LT films. This is largely caused by the higher surface mobility during deposition. Furthermore, the film surface is very rough, and the CdTe grains are highly faceted. Despite the dramatic increase in grain size, little improvement was observed in the electrical properties of the films. This suggests that although the grain boundary density is lower in HT films, strong carrier recombination (caused by a high density of electrical recombination centers) is still dominant.

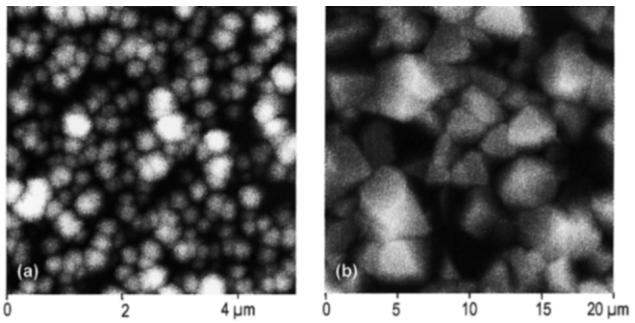

Fig. 1. AFM images of CdTe films deposited at: (a) 450°C; and (b) 620°C.

Fig. 2 shows the evolution of the morphology as a

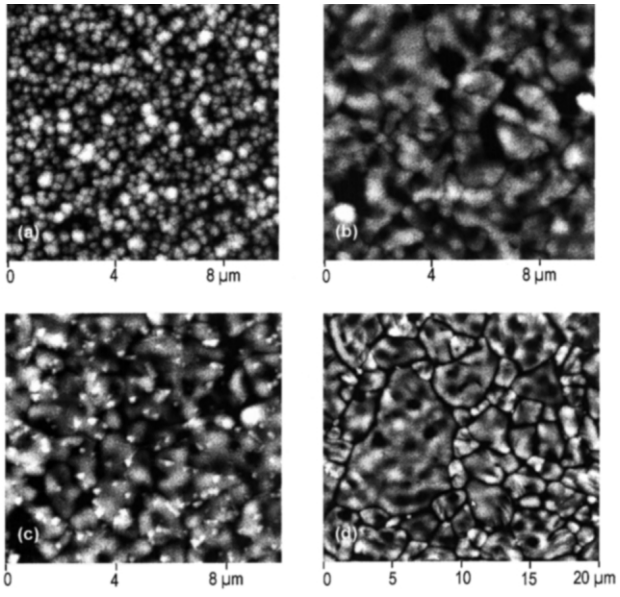

Fig. 2. AFM images of CdTe films deposited at 450°C: (a) as-deposited; (b) heat-treated at 400°C; (c) heat-treated at 420°C; and (d) heat-treated at 450°C.

Table 1
Efficiency of CdTe solar cells deposited by close-spaced sublimation at 450°C and processed under different conditions

Reference	Post-deposition treatment	Efficiency (%)
P2195	Vapor $CdCl_2$, 425°C, 5 min	10.1
P2181	Vapor $CdCl_2$, 430°C, 5 min	11.6
P2197	Vapor $CdCl_2$, 435°C, 5 min	8.3
P2184	Vapor $CdCl_2$, 450°C, 5 min	6.7

function of vapor $CdCl_2$ treatment. The treatment conditions were kept constant, while the treatment temperature was varied from 400 to 450°C. Bearing in mind that the average grain size is 0.3 μm in as-deposited films (Fig. 2a), significant grain growth was observed for samples treated at 400°C, resulting in a grain size of 1.3 μm (Fig. 2b). Fig. 2 clearly reveals that the grain growth continued as the treatment temperature was increased to 450°C, yielding a grain size of approximately 4.4 μm (Fig. 2d). We have also observed that this vapor treatment is more effective in recrystallization than the commonly used dipping process. This is likely due to the fact that, during the vapor process, an infinite supply of Cl is available, whereas in the dipping process the amount of Cl is limited to the residual layer on the film surface. It is also worth pointing out that the dipping treatment is carried out for at least 30 min, whereas the duration of the vapor treatment is only 5 min.

The microstructure of these films was found to depend strongly on the deposition and heat-treatment temperatures. Plan-view TEM examination of LT films (Fig. 3a) confirmed the AFM findings of small-grain morphology and revealed a high density of intra-grain dislocations. The density of these dislocations, however, varied from one grain to another. HT films, on the other hand, exhibited a much lower density of dislocations, but a high density of planar faults was observed. The evolution of the microstructure of LT films with heat treatment was studied by detailed TEM examination. As the treatment temperature increases, the dislocation density decreases, while the planar fault density increases. At a treatment temperature of 430°C, the microstructure is very similar to that of as-deposited HT films.

Particular emphasis was placed in this study on the high-resolution transmission electron microscopy (HRTEM) characterization of planar faults in CdTe films. We found that these extended defects are mostly lamellar twins and stacking faults with similar densities. Fig. 4 shows a typical HRTEM image of these defects, with the electron beam parallel to the $[1\bar{1}0]$ zone axis. The planar defects are indicated by white arrows, while

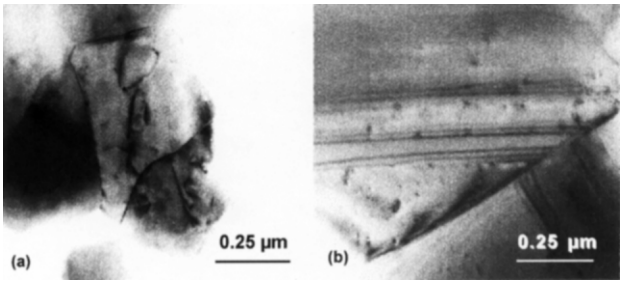

Fig. 3. TEM plan-view of CdTe films deposited at: (a) 450°C; and (b) 620°C.

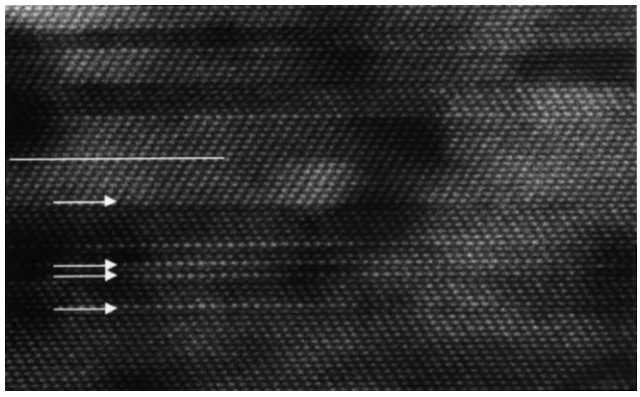

Fig. 4. HRTEM image showing a high density of planar defects lying on {111} planes.

the white solid line in the figure indicates a {111} plane of CdTe. This image clearly shows that the planar defects have a {111} habit plane.

CdTe normally possesses a zincblende structure that can be described by the stacking of close-packed double layers of {111} planes in the ⟨111⟩ direction. The normal, perfect stacking sequence is …AaBbCcAaBbCc…, where each letter represents a stacking plane. Introducing any error to the perfect stacking sequence will result in a planar defect. The most common planar defects are the so-called lamellar twin, which is produced by inverting the stacking sequence, and the intrinsic and extrinsic stacking faults, produced by removing or adding a double layer, respectively.

Fig. 5 shows higher-magnification HRTEM images revealing the details of stacking faults lying on {111} planes, as indicated by the lines. In Fig. 5a, the two sides of the stacking fault have the same orientation, which is clearly different from a lamellar twin. A displacement along the $[11\bar{2}]$ direction on the (111) plane is seen from the image, indicating that this is likely to be an intrinsic stacking fault. The inset is the simulated image of the intrinsic stacking-fault model, at a defocus of −60 nm for a thickness of 10 nm. The good match provides strong evidence that the defect shown in Fig.

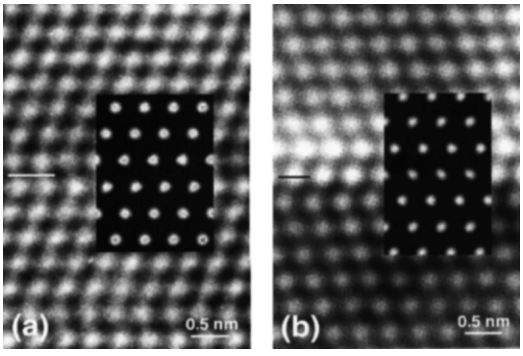

Fig. 5. $[1\bar{1}0]$ zone axis HRTEM images of an: (a) intrinsic stacking fault; and (b) extrinsic stacking fault. The insets are the simulated images of the structure models.

5a is an intrinsic stacking fault with a displacement of $R = \frac{1}{6}[11\bar{2}]$.

Fig. 5b shows a HRTEM image of a different planar defect. Like the intrinsic stacking fault, the two sides of this defect have the same orientation, implying that this is a stacking fault. However, unlike the intrinsic stacking fault, there is an intermediate layer in between the two sides of the fault, as indicated by the black line. This clearly indicates that this defect is an extrinsic stacking fault. The inset is the simulated image of the extrinsic stacking-fault model, at a defocus of −60 nm for a thickness of 10 nm. The simulated image is an excellent fit for the HRTEM image, demonstrating that the defect shown in Fig. 5b is an extrinsic stacking fault.

The bonding arrangement across the lamellar twins and stacking faults are very similar, i.e., no wrong bonds (of the Cd–Cd or Te–Te type) or dangling bonds across the twin boundary. Hence, both lamellar twins and stacking faults have a very low formation energy. We believe that this is the reason why lamellar twins and stacking faults with similar densities are often observed in these CdTe thin films. More importantly, we observed that these extended defects can often form closely spaced arrangements, leading to a local phase transformation from the cubic structure to a hexagonal structure. As indicated above, the lamellar twins and the intrinsic and extrinsic stacking faults only introduce a change in the stacking sequence. Therefore, the closely spaced arrangement of these defects will change the stacking sequence from that of a cubic structure, …AaBbCc…, to that of a hexagonal structure, …AaBbAaBb..., leading to a hexagonal structure sandwiched between two cubic CdTe regions. The band structure of the zincblende and hexagonal structures of many semiconductors has been discussed in detail previously [10,11]. The bandgap of hexagonal CdTe is slightly larger than that of cubic CdTe. Due to the offset between the valence band maxima of these two structures, the presence of the hexagonal phase is expected to have considerable effects on the electrical properties of the CSS-grown polycrystalline CdTe films. This topic is discussed in more detail in a related paper by Yan et al. [12].

The recombination dynamics of grain boundaries in LT CdTe was examined by plan-view CL measurements with electron-beam injection at the free CdTe surface. To enable us to correlate the CL and secondary electron (SE) images, CL linescans were superimposed on the SE micrographs. A systematic local decrease in the excited panchromatic CL emission was detected whenever the e-beam scanned across a grain boundary (GB). The resulting dark contrast at the GBs in the CL images indicates higher non-radiative recombination efficiency at the GBs. Fig. 6 shows the contrast from CL linescans recorded at different e-beam currents of

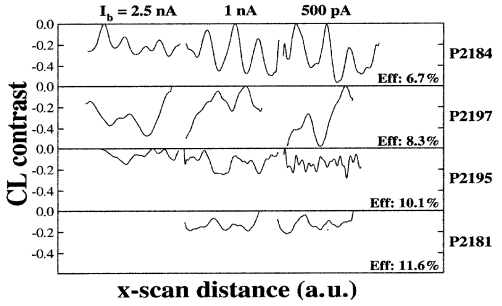

Fig. 6. Panchromatic CL contrast from grain boundaries in LT CdTe cells recorded at different electron-beam currents of 500 pA, and 1 and 2.5 nA. Clearly, the lower the CL contrast, the higher the cell efficiency.

500 pA, and 1 and 2.5 nA. For LT CdTe films, the cell efficiency is maximal at a post-deposition treatment temperature of 430°C and is degraded at higher treatment temperatures (Table 1). By analyzing Fig. 6, the efficiency of the solar cells can be clearly correlated with the CL contrast, which is lower at higher cell efficiencies. Indeed, higher non-radiative recombination rates at GBs lead to stronger CL contrast. This effect suggests that recombination at GBs in CdTe thin films plays a major role in cell performance. Furthermore, the degree of GB passivation is a function of the post-deposition temperature for the same as-grown cell.

4. Summary

The morphology, microstructure, and luminescent properties of polycrystalline CdTe films were investigated. Films deposited at low temperature exhibited fine (0.3 μm), equiaxed grains. Dramatic grain growth was observed as a consequence of heat treatment. The $CdCl_2$ vapor treatment used in this work proved to be more effective than the conventional solution approach. The film microstructure is heavily faulted and strongly dependent on the deposition and post-deposition treatment temperatures. Films deposited at low temperature exhibited a high density of intra-grain dislocations. However, after heat treatment, the microstructure was dominated by planar defects. Similar results were obtained from films deposited at high temperature. The planar defects were mostly lamellar twins and stacking faults with similar densities. Furthermore, these defects often formed a closely spaced arrangement, leading to the formation of localized hexagonal phases buried in the cubic CdTe phase. CL investigations focused on the recombination behavior of grain boundaries as a function of heat treatment. The recombination efficiency of these boundaries decreased with increasing temperature up to 430°C, after which a significant degradation was observed. This correlated well with cell efficiency measurements.

Acknowledgements

This work was supported by the U.S. Department of Energy under Contract No. DE-AC36-99GO10337.

References

[1] J. Britt, C. Ferekides, Appl. Phys. Lett. 62 (1993) 2851.
[2] H.M. Al-Allak, A.W. Brinkman, H. Richter, D. Bonnet, J. Cryst. Growth 159 (1996) 910.
[3] B.E. McCandless, L.V. Moulton, R.W. Birkmire, Prog. Photovolt. 5 (1997) 249.
[4] M.M. Al-Jassim, R.G. Dhere, K.M. Jones, F.S. Hasoon, P. Sheldon, in: J. Schmid, H.A. Ossenbrink, P. Helm, H. Ehmann, E.D. Dunlop (Eds.); Proceedings of 2nd World Conference on Photovoltaic Solar Energy Conversion, European Commission, Italy, pp. 1063–1066.
[5] D.J. Smith, S.-C.Y. Tsen, Y.P. Chen, J.-P. Faurie, S. Sivananthan, Appl. Phys. Lett. 67 (1995) 1591.
[6] Y. Xin, N.D. Browning, R. Rujirawat, S. Sivananthan, Y.P. Chen, P.D. Nellist, S.J. Pennycook, J. Appl. Phys. 84 (1998) 4292.
[7] R.G. Dhere, D.S. Albin, D.H. Rose, S.E. Asher, K.M. Jones, M.M. Al-Jassim, Mater. Res. Soc. Proc. 426 (1996) 361.
[8] S.A. Galloway, P.R. Edwards, K. Durose, Inst. Phys. Conf. Ser. 157 (1997) 579.
[9] S.A. Galloway, A.J. Holland, K. Durose, J. Cryst. Growth 159 (1996) 925.
[10] C.-Y. Yeh, S.-H. Wei, A. Zunger, Phys. Rev. B 50 (1994) 2715.
[11] T. Mattila, S.-H. Wei, A. Zunger, Phys. Rev. Lett. 83 (1999) 2010.
[12] Y. Yan, M.M. Al-Jassim, K.M. Jones, S.-H. Wei, S.B. Zhang, Appl. Phys. Lett. 77 (2000) 1461.